

# Globular clusters and supermassive black holes in galaxies: further analysis and a larger sample

Gretchen L. H. Harris<sup>1\*</sup> Gregory B. Poole<sup>2</sup> and William E. Harris<sup>3</sup>

<sup>1</sup>*Department of Physics and Astronomy, University of Waterloo, Waterloo ON N2L 3G1, Canada*

<sup>2</sup>*School of Physics, University of Melbourne, Parkville, Victoria 3010, Australia*

<sup>3</sup>*Department of Physics and Astronomy, McMaster University, Hamilton ON L8S 4M1, Canada*

Accepted Received; in original form

## ABSTRACT

We explore several correlations between various large-scale galaxy properties, particularly total globular cluster population ( $N_{GC}$ ), the central black hole mass ( $M_{\bullet}$ ), velocity dispersion (nominally  $\sigma_e$ ), and bulge mass ( $M_{dyn}$ ). Our data sample of 49 galaxies, for which both  $N_{GC}$  and  $M_{\bullet}$  are known, is larger than used in previous discussions of these two parameters and we employ the same sample to explore all pairs of correlations. Further, within this galaxy sample we investigate the scatter in each quantity, with emphasis on the range of published values for  $\sigma_e$  and effective radius ( $R_e$ ) for any one galaxy. We find that these two quantities in particular are difficult to measure consistently and caution that precise intercomparison of galaxy properties involving  $R_e$  and  $\sigma_e$  is particularly difficult.

Using both conventional  $\chi^2$  minimization and Monte Carlo Markov Chain (MCMC) fitting techniques, we show that quoted observational uncertainties for all parameters are too small to represent the true scatter in the data. We find that the correlation between  $M_{dyn}$  and  $N_{GC}$  is stronger than either the  $M_{\bullet}$  -  $\sigma_e$  or the  $M_{\bullet}$  -  $N_{GC}$  relations. We suggest that this is because both the galaxy bulge population and  $N_{GC}$  were fundamentally established at an early epoch during the same series of star-forming events. By contrast, although the seed for  $M_{\bullet}$  was likely formed at a similar epoch, its growth over time is less similar from galaxy to galaxy and thus less predictable.

**Key words:** galaxies: black holes, globular clusters, fundamental parameters

## 1 INTRODUCTION

As the available database describing the global properties of individual galaxies has grown, it has become increasingly feasible to try to understand more about these systems by exploring correlations among several large-scale structural parameters. These global parameters often include:  $\sigma_e$  (bulge velocity dispersion),  $M_{dyn}$  (bulge mass as calculated through the virial theorem or its variants),  $R_e$  (effective radius),  $\mu_e$  (mean surface brightness), luminosity, and more recently  $M_{\bullet}$  (mass of the central supermassive black hole). One of the earliest demonstrations of such correlations was the work of Djorgovski and Davis (1987) who used a sample of 260 systems to show that early-type galaxies form a two-parameter family characterized by velocity dispersion and mean surface brightness, introducing the concept of a fundamental plane for galaxies. Correlations

with  $M_{\bullet}$  properties were first constructed by Kormendy & Richstone (1995) (8 galaxies) and Magorrian et al. (1998) (36 galaxies). Since then, Ferrarese & Merritt (2000) and Gebhardt et al. (2000) demonstrated a correlation between  $M_{\bullet}$  and  $\sigma_e$ , which appeared to have lower dispersion than the relation between  $M_{\bullet}$  and the luminosity of the galactic bulge or other parameters. However, the slopes of the  $M_{\bullet}$ - $\sigma_e$  relation derived by these two groups were significantly different and the debate on this point continues energetically today (e.g. Merritt & Ferrarese 2001; Tremaine et al. 2002; Novak et al. 2006; Graham et al. 2011; Gültekin et al. 2011a, to cite a few).

Recently, Spitler & Forbes (2009) proposed links among a galaxy’s globular cluster system (GCS), total halo mass, and SMBH mass. From a sample of 13 galaxies, Burkert & Tremaine (2010) (hereafter BT) also showed that  $M_{\bullet}$  is almost directly proportional to the total globular cluster population of a galaxy,  $N_{GC}$ . At first glance the statement that  $N_{GC} \sim M_{\bullet}$  should not be thought of as terribly surprising, since both  $N_{GC}$  and  $M_{\bullet}$  are known to be related to other

\* E-mail: ghharris@astro.uwaterloo.ca; gregory.poole@unimelb.edu.au; harris@physics.mcmaster.ca

galaxy properties such as mass and luminosity (see especially Harris et al. (2013) (hereafter HHA13) for a recent comprehensive discussion of GC populations and systematics); essentially, larger galaxies should on average have more massive SMBHs and more globular clusters. But more interesting, and possibly more important for understanding early galaxy evolution, is the suggestion that the *scatter* in the  $M_{\bullet} - N_{GC}$  correlation is remarkably small, comparable with or even lower than what has been claimed for  $M_{\bullet}$  vs.  $\sigma_e$ . The low scatter is harder to explain by trivial scaling arguments, and is what makes this newly-found correlation intriguing.

Harris & Harris (2011) (hereafter HH) confirmed the findings of Spitler & Forbes (2009) and BT from a much larger sample of 33 galaxies with well determined  $N_{GC}$  and  $M_{\bullet}$  values. They found, as did BT but with stronger confidence, that  $M_{\bullet}$  scales nearly linearly with  $N_{GC}$  ( $M_{\bullet} \sim N_{GC}^{0.98 \pm 0.10}$ ) and also drew attention to a number of other issues:

- Occasional genuine outliers that fall well off the central  $N_{GC} - M_{\bullet}$  relation cannot be explained by measurement uncertainties in either quantity. Most notably, the Milky Way and NGC 5128 are both strong outliers in the sense that they have too-small SMBH's for their number of GCs, though both quantities are well determined.

- The residual scatter around the mean relation  $M_{\bullet} \sim N_{GC}$  is very noticeably larger than expected from the random measurement uncertainties quoted in the literature, suggesting that the scatter is dominated by a real cosmic variance.

- The spiral galaxies (with the exception of the Milky Way) follow the E-galaxy relation quite closely. By contrast, the S0 galaxies in the list show much larger scatter and no well defined slope; for them, the basic E/S relation “appears to be irrelevant”.

Additional recent discussions of the correlations between the GCS and the SMBH have been published by Snyder et al. (2011), Sadoun & Colin (2012), and Rhode (2012). Snyder et al. (2011) argue essentially that the relatively low scatter in  $M_{\bullet} - N_{GC}$  can be interpreted by seeing both quantities as linked to (and perhaps determined by) the galaxy's bulge mass. Sadoun & Colin (2012) extend the discussion to propose a correlation between  $M_{\bullet}$  and the velocity dispersion of the globular cluster system,  $\sigma_{GCS}$ ; at present, this interesting relation can be built on only 13 large galaxies with available GCS velocity data.

Rhode (2012) selected 20 galaxies (10E, 8S0, and 2S) with particularly complete, homogeneous GCS data and found  $M_{\bullet} \sim N_{GC}^{1.20 \pm 0.06}$ , a  $\sim 20\%$  steeper slope than in HH. The steeper slope seems primarily to be due to her use of only large galaxies in the fit (essentially Milky-Way-sized and larger), whereas HH used galaxies over the entire existing luminosity range, including dwarfs. HH also include two very luminous E's, M87 and NGC 5846, that Rhode does not. These extreme cases at the top end and bottom end of the correlation make up only a minority of the total sample but they exert strong leverage over the fit. It is not out of the question that with much more, and more precise, data in hand the  $N_{GC} - M_{\bullet}$  relation might appear slightly nonlinear. Notably, Rhode (2012) also finds that the slope does not change significantly if the GC sample is subdivided into its blue (metal-poor) and red (metal-richer) subpopu-

lations, a step that can be done only for high-quality GCS photometry in which the division between red and blue can be clearly made. As in HH, she also found that the S0 and disk galaxies in this selected sample showed larger scatter than the E's (though still based on a very small sample).

In this paper, we explore the various correlations of these global parameters for a still larger sample of galaxies, paying the closest attention to four of the ones listed above:  $M_{\bullet}$ ,  $N_{GC}$ ,  $\sigma_e$ , and  $M_{dyn}$ . We find that the relation with the smallest scatter of all is the one between  $N_{GC}$  and the dynamical bulge mass,  $M_{dyn}$ , and suggest a possible evolutionary link between them. We have two additional objectives. First, we directly compare best-fit solutions from a conventional  $\chi^2$ -minimization procedure, with ones obtained from a MCMC (Monte Carlo Markov Chain) technique. Second, we discuss the residual scatters around these solutions in an attempt to decide whether or not we have already resolved the intrinsic (cosmic) scatter in the parameters.

## 2 CAUSAL CONNECTIONS?

The SMBH of a galaxy is a structural feature with a typical size of a few AU, whereas the GCS spans tens to hundreds of kiloparsecs, a factor of  $10^{10}$  bigger in scale size. So a *causal* link between the SMBH and the globular cluster population may therefore seem quite unlikely. But the possibility should not simply be dismissed out of hand. HH pointed out that both the SMBH and GCS have their origins in the same earliest phases of galaxy formation at  $z \sim 5 - 10$ . There is a rich literature on how SMBH-driven AGN activity can strongly influence star formation in large galaxies through either negative or positive feedback, particularly in the high-redshift stages when the most gas is present (Silk & Rees 1998; Fabian 2012). To cite only a few recent examples, Wagner et al. (2012, 2013) present models of AGN jets interacting with a fractal-like ISM in the central kpc. These show that a high fraction of the jet energy is transferred to the gas, and also that the jet can quickly ( $< 10^6$  y) penetrate through the central bulge out into the halo regions by channeling through the intercloud regions. Lower-density regions of the gas are ablated and heated by the jet, but the densest gas cores (among which would be protoglobular clusters) are preserved. In addition, the star formation rate outside the central region will be enhanced through AGN ram compression (Fabian 2012; Gaibler et al. 2012; Silk 2005; Ishibashi & Fabian 2012). Once the powerful jet penetrates into the halo, its energy can be deposited and percolated over many-kiloparsec scales within a few  $10^8$  years, an appropriate time period for the formation of the first GCs.

On the observational side, AGN- or QSO-driven star formation in galaxies at  $z \sim 2 - 3$  seems able to occur in sites many tens of kpc from the galaxy center (e.g. Rauch et al. 2013; Croft et al. 2006; Klammer et al. 2004; Bicknell et al. 2000, among many others). Most of the discussions on jet-influenced star formation so far have concentrated on the global properties of their host galaxies. It remains to be seen whether or not GC formation can be either inhibited or enhanced relative to field-star formation by AGN activity.

An opposite approach, that GCs can *build* or at least enlarge the central SMBH, has been promoted in other recent papers (see, e.g. Capuzzo-Dolcetta & Donnaruma

2001; Capuzzo-Dolcetta & Vicari 2005; Capuzzo-Dolcetta & Mastrobuono-Battisti 2009, for comprehensive discussions). The essential idea is that GCs in the inner region of a galaxy can be disrupted by dynamical friction over a timescale short enough to add significantly to the stellar population of the central bulge (Tremaine et al. 1975) and thus, perhaps, to the central black hole as well. Their quantitative estimates are based on the assumption that the radial distribution of GCs in the galaxy was initially the same as the distribution of field-star light, and that it is now flatter in the central regions because GCs there were destroyed. Under this assumption typically 30-50% of the original GC population may have been lost this way. Plotting SMBH mass versus the *calculated* mass from the supposedly “lost” clusters then shows a very rough positive correlation (Capuzzo-Dolcetta & Donnaruma 2001; Capuzzo-Dolcetta & Mastrobuono-Battisti 2009). Significant difficulties confront this interpretation. It invokes a large number of long-vanished (and massive) GCs, and to make a major contribution to the SMBH growth, very large numbers of stars from the disrupted GCs would have to find their way into a tiny, AU-sized central black hole rather than just joining the bulge stellar population. Another traditional objection to such a picture is that the innermost bulge population is generally much more metal-rich (reaching Solar or higher; e.g. Johnson et al. 2013) than all but a few individual GCs (which mostly range from 1/3 to 1/200 Solar), so only a small fraction of the bulge can have been built by cluster disruption. Furthermore, there is no evidence that even the most massive GCs in existence ( $10^7 M_\odot$  and above) are sufficiently metal-rich to match the inner bulge population (Harris, W. 2009).

Yet another approach would be to assume that intermediate-mass BHs already residing in the GCs could combine to add to the galaxy’s SMBH. Little is known about the presence or actual masses of IMBHs though they have been proposed as seeds for SMBH formation (see, e.g. Jalali et al. 2012, for a recent discussion). One of the best observational cases for an IMBH is in  $\omega$  Centauri, for which plausible evidence exists that an IMBH of  $50,000 M_\odot$  is present (Jalali et al. 2012). If we suppose that (a) all GCs contain IMBHs, (b) their IMBH mass is directly proportional to cluster mass with a mass ratio of 2% like  $\omega$  Cen, and (c) all the IMBHs in the disrupted GCs add to the central SMBH, then on the average 1000 GCs (a typical value for a moderately large elliptical) could add  $\sim 5 \times 10^6 M_\odot$  to the SMBH. All of these assumptions are arbitrary, and in any case this added mass is only a few percent of the typical  $\sim 10^8 M_\odot$  SMBH mass for the same type of galaxy (see below).

Recently, Jahnke and Maccio (2011) explored the very different possibility, suggested by Peng (2007), that the origin of the  $M_\bullet - M_{bulge}$  (equivalent to our  $M_{dyn}$ ) relation results from a statistical convergence process rather than a causal, physical one. They used numerical simulations and merger trees to demonstrate that hierarchical galaxy formation leads to a linear relation between SMBH and bulge mass even if their initial distributions were strongly uncorrelated. The initial  $M_\bullet - M_{bulge}$  correlation they derived from this simple assumption was, however, much tighter than is observed and had a different slope. By adding other features to their simulations (including star formation, black hole accretion, and disk to bulge mass conversion) they produced correlations much more similar to observed data and

concluded that the relation “is produced naturally by the merger-driven assembly of bulge and BH mass, and without any coupling of SF and BH mass growth per individual galaxy”.

Our conclusion for the present is that the likeliest chance to establish a causal link between the GCS and SMBH (if there is one) would be through AGN feedback and its influence on star and GC formation. Much ground remains to be explored in this direction through modelling. The possibility of a noncausal, statistical origin also remains competitive.

### 3 THE DATA

In a parallel study, HHA13 have compiled a catalog of 422 galaxies of all types with  $N_{GC}$  data published to the present time. Among these there are now 49 galaxies with measurements of both  $M_\bullet$  and  $N_{GC}$ : 34 ellipticals (E), 10 “lenticulars” (S0), and 5 spirals (S). As discussed by HH, the dominance of E galaxies in our sample is partly because more central black hole masses are known for ellipticals, but partly because the best S0 and S galaxies in which to determine  $M_\bullet$  are face-on or nearly so. By contrast,  $N_{GC}$  studies in disk galaxies are best done for edge-on systems, minimizing the disk contamination and background light. Thus for disk galaxies, the globular cluster studies and SMBH studies in the literature have traditionally had little overlap. The situation for the E’s is much better.

As hinted above, a primary issue in interpreting the correlations that we derive in the discussion below is that the dispersions (rms scatters) found around the best-fit relations are consistently larger than expected from the formal errors quoted in the literature for the individual measured parameters. Before proceeding with our correlation solutions, therefore, we (1) discuss just what typical ranges of values have been found in different studies for each key quantity, and (2) develop as self-consistent a database as possible for our sample. We discuss in turn the data for galaxy distance, effective radius, velocity dispersion,  $N_{GC}$ , and bulge mass and  $M_\bullet$ .

#### 3.1 Distance

As noted above, we are primarily interested in galaxies where both  $M_\bullet$  and  $N_{GC}$  are measured and our final adopted list is in Table 1. Not surprisingly, these are in cosmologically nearby space and so also have published measurements of  $\sigma_e$  and  $R_e$  from which their dynamical masses  $M_{dyn}$  can be directly calculated once the distance is known. However, because their distances range from less than 1Mpc to more than 100Mpc the best available distances are themselves based on a variety of techniques. As a result, it is not feasible to apply any single distance method to the whole sample. Because  $R_e$ ,  $M_{dyn}$ , and  $M_\bullet$  all scale with distance, we chose first to assess distance values for each galaxy individually.

The distances quoted in Table 1 are based on three methods: stellar standard candles, surface brightness fluctuations (SBF), and redshift (i.e. Hubble’s law). For the six galaxies nearer than 4Mpc it is possible to resolve individual stars and use standard candles such as RR Lyrae stars, Cepheids, and the luminosity of the tip of the red giant

**Table 1.** Selected Global Properties of Galaxies

Galaxy	Type	d (Mpc)	$N_{GC}(\pm)$	$\log M_{BH}/M_{\odot}(\pm)$	$\sigma_e(\pm)$ (km/s)	$R_e$ (kpc)	$\log (M_{dyn}/M_{\odot})$	References
MilkyWay	Sbc	0.0	160 (10)	6.61(+0.04,-0.04)	105(20)	0.70	9.73	2,3,4
NGC221	E2	0.8	1 (9)	6.46(+0.08,-0.10)	75( 3)	0.15	8.77	2,5,6,7,8
NGC224	Sb	0.7	450 (100)	8.18(+0.20,-0.10)	160( 8)	1.06	10.28	9,10,11,12,13,14
NGC253	SBc	3.4	20 (10)	7.00(+0.30,-0.30)	109( 5)	0.31	9.41	15,16 17,18
NGC821	E4	24.1	320 (40)	8.23(+0.16,-0.25)	209(10)	5.32	11.20	19,20
NGC1023	SB0	11.4	221 (100)	7.64(+0.04,-0.04)	205(10)	1.98	10.76	21,22
NGC1316	E	21.5	647 (100)	8.24(+0.17,-0.23)	226( 9)	3.75	11.12	23,24,25
NGC1332	S0	22.9	1000 (500)	9.17(+0.06,-0.06)	328(16)	0.93	10.82	1,26,27
NGC1399	E1	20.0	6625(1180)	8.69(+0.06,-0.07)	337(16)	4.11	11.51	28,29,30,31
NGC2778	E2	22.9	50 (30)	7.15(+0.30,-0.30)	175( 8)	1.83	10.59	2,32,20
NGC3031	Sb	3.6	172 (100)	7.84(+0.11,-0.06)	143(16)	1.74	10.39	33,34
NGC3115	S0	9.7	550 (150)	8.96(+0.19,-0.15)	230(11)	1.70	10.79	35,36
NGC3377	E5	11.2	266 (66)	8.25(+0.19,-0.29)	145( 7)	1.83	10.43	26,01
NGC3379	E1	10.6	270 (68)	8.04(+0.22,-0.26)	206(10)	1.80	10.73	37,38
NGC3384	SB0	11.6	128 (100)	7.04(+0.16,-0.26)	143( 7)	0.73	10.02	37,20
NGC3414	S0	25.2	400 (200)	9.40(+0.06,-0.08)	205(11)	4.1	11.08	26,57,69
NGC3585	S0	20.0	300 (100)	8.51(+0.15,-0.13)	213(10)	3.83	11.08	1,39,40
NGC3607	E	22.8	600 (200)	8.15(+0.10,-0.15)	229(11)	7.25	11.42	1,26,40
NGC3608	E2	22.9	450 (200)	8.67(+0.09,-0.10)	182( 9)	3.91	10.96	1,26,20
NGC3842	E	98.4	9850(3900)	9.99(+0.11,-0.13)	270(14)	17.8	11.96	1,41,42
NGC4261	E2	31.6	530 (100)	8.71(+0.08,-0.09)	315(15)	5.92	11.61	2,43,44
NGC4291	E2	26.2	1200 (600)	8.98(+0.10,-0.18)	242(12)	1.87	10.88	1,26,20
NGC4350	S0	15.4	196 (60)	8.74(+0.10,-0.10)	175( 5)	1.37	10.47	45,46
NGC4374	E1	18.4	4300(1200)	8.96(+0.05,-0.04)	296(14)	4.87	11.47	45,47
NGC4382	E2	18.4	1100 (181)	7.81(upper limit)	182( 5)	6.37	11.17	45,48
NGC4459	E2	16.1	218 (28)	7.84(+0.08,-0.08)	167( 8)	1.16	10.35	45,49
NGC4472	E2	16.3	7800 (850)	9.26(+0.12,-0.18)	310(10)	8.22	11.74	45,50
NGC4473	E5	15.7	376 (97)	7.95(+0.19,-0.29)	190( 9)	1.90	10.67	45,20
NGC4486	E0	16.1	13300(2000)	9.77(+0.03,-0.03)	324(16)	7.80	11.76	45,51,52
NGC4486A	E2	15.6	11 (12)	7.15(+0.13,-0.11)	111( 5)	0.53	9.66	45,53
NGC4486B	E1	16.3	4 (11)	9.00(upper limit)	185( 9)	0.24	9.76	45,54
NGC4552	E1	15.3	1200 (250)	8.68(+0.04,-0.05)	233(11)	2.20	10.92	45,51,55
NGC4564	S0	15.0	213 (31)	7.92(+0.10,-0.14)	162( 8)	1.58	10.46	45,20
NGC4594	Sa	9.8	1900 (300)	8.72(+0.30,-0.57)	240(12)	2.53	11.01	19,56
NGC4621	E4	18.3	800 (355)	8.60(+0.06,-0.07)	225(11)	4.12	11.16	45,57
NGC4649	E2	16.8	4745(1100)	9.63(+0.09,-0.11)	385(19)	7.30	11.88	45,20
NGC4697	E6	11.7	229 (50)	8.28(+0.08,-0.10)	177( 8)	4.27	10.97	45,20
NGC4889	E	103.2	11000(1340)	10.32(+0.25,-0.54)	347(17)	25.1	12.32	58,42
NGC5128	E0p	3.8	1300 (300)	7.71(+0.13,-0.19)	150( 7)	5.60	10.94	59,55,60,61
NGC5813	E2	32.2	1650 (400)	8.84(+0.07,-0.07)	239(12)	7.60	11.48	62,57
NGC5845	E3	25.9	140 (70)	8.69(+0.12,-0.16)	234(11)	0.51	10.29	1,26,20
NGC5846	E0	24.9	4700(1200)	9.04(+0.07,-0.09)	237(12)	9.97	11.59	63,57
NGC6086	E	132.0	4584(1362)	9.56(+0.16,-0.16)	318(16)	20.30	12.16	1,64,42
NGC7332	S0	23.0	175 (15)	7.11(+0.17,-0.21)	116( 6)	1.2	10.05	70,57
NGC7457	S0	13.2	178 (75)	7.00(+0.20,-0.40)	67( 3)	0.90	9.45	65,20
NGC7768	E	112.8	3000(1300)	9.11(+0.15,-0.27)	257(13)	12.6	11.76	64,71,42
IC1459	E4	29.2	2000 (800)	9.45(+0.14,-0.25)	340(17)	5.47	11.64	1,26,55
IC4296	BCG	50.8	6400(1600)	9.13(+0.06,-0.07)	322(12)	10.20	11.86	1,66,67
A2052	BCG	141.0	27000(9000)	9.66(upper limit)	233(11)	38.30	12.16	68,67

Sources: (1) This paper, (2) Harris & Harris (2011), (3) Ghez et al. (2008), (4) Gillessen et al. (2009), (5) Lee et al. (2008), (6) Verolme et al. (2002), (7) Grillmair et al. (1996), (8) Fiorentino et al. (2010), (9) Battistini et al. (1993), (10) Bender et al. (2005), (11) Ferrarese et al. (2006), (12) Brown et al. (2004), (13) McConnachie et al. (2005), (14) Sarajedini et al. (2009), (15) Olsen et al. (2004), (16) Rodriguez-Rico et al. (2006), (17) Dalcanton et al. (2009), (18) Rekola et al. (2005), (19) Spitler et al. (2008), (20) Schulze & Gebhardt (2011), (21) Larsen & Brodie (2000), (22) Bower et al. (2001), (23) Villegas et al. (2010), (24) Richtler et al. (2012), (25) Nowak et al. (2008), (26) Kundu & Whitmore (2001), (27) Rusli et al. (2011), (28) Bassino et al. (2006), (29) Dirsch et al. (2003), (30) Houghton et al. (2006), (31) Gebhardt et al. (2007), (32) Gebhardt & Kissler-Patig (1999), (33) Santiago-Cortés et al. (2010), (34) Djorgovski and Davis (1987), (35) Hanes & Harris (1996), (36) Emsellem et al. (1999), (37) Harris & van den Bergh (1981), (38) Gebhardt et al. (2000), (39) Puzia et al. (2004), (40) Gültekin et al. (2009a), (41) Butterworth & Harris (1992), (42) McConnell et al. (2011), (43) Giordano et al. (2005), (44) Ferrarese et al. (1996), (45) Peng et al. (2008), (46) Pignatelli et al. (2001), (47) Bower et al. (1998), (48) Gültekin et al. (2011b), (49) Sarzi et al. (2001), (50) Shen & Gebhardt (2010), (51) Tamura et al. (2006), (52) Gebhardt et al. (2011), (53) Nowak et al. (2007), (54) Kormendy et al. (1997), (55) Cappellari et al. (2009), (56) Kormendy (1988), (57) Graham (2008), (58) Harris et al. (2009), (59) Harris, G.L.H. (2010), (60) Neumayer (2010), (61) Harris et al. (2010), (62) Hopp et al. (1995), (63) Forbes et al. (1997), (64) Blakeslee et al. (1997), (65) Chomiuk et al. (2008), (66) Okon & Harris (2002), (67) Dalla Bontà et al. (2009), (68) Harris et al. (1995), (69) Hu (2008), (70) Forbes, Georgakakis, & Brodie (2001), (71) Jordán, A. et al. (2004)

branch, with resulting uncertainties of  $\sim 5\%$ . SBF distances are available for the great majority of our sample and we use them for the galaxies between 4 Mpc and 50 Mpc; formal SBF uncertainties range from  $\sim 4\text{--}15\%$ . For five galaxies beyond  $\sim 50$  Mpc, we use the galaxy’s redshift relative to the cosmic microwave background (CMB) and  $H_o = 70 \pm 2$  km/s/Mpc. Formal uncertainties for the most distant galaxies in our sample are  $\sim 7\%$ .

Since publication of the first major SBF sample by Tonry et al. (2001), the calibration has been revised several times. Jensen et al. (2003) used Hubble Space Telescope (HST) *IR* imaging to study 65 galaxies while Blakeslee et al. (2009) recalibrated distances for 134 galaxies in the Virgo and Fornax clusters, again with HST. Unfortunately for our purposes, neither of these had more than a 50% overlap with our sample. For the galaxies in Tonry et al. (2001) in common between Jensen et al. (2003) or Blakeslee et al. (2009) we find a mean difference of  $\Delta(m - M)_0(T - B/J) = 0.16 \pm 0.10$ . Given the lack of compelling evidence to support any large adjustment to the Tonry et al. (2001) values, which overlap with  $\sim 85\%$  of our sample, we have chosen to use the 2001 distances here.

McConnell et al. (2011) use redshift-based distances with  $H_o = 70$  for all of the galaxies in their compilation and, given the mix of distance methods we have applied, it is useful to compare the two datasets for the 39 galaxies in common. In Figure 1 we compare their redshift distances with our resolved-star and SBF values. As seen in the top panel, the distance difference ( $d - d_z$ ) is, on average, less than the formal error in the stellar/SBF distances. In addition (lower panel), the redshift distances are systematically larger, although within the errorbars shown.

For most of the following discussion we will use the mainly non-redshift distances given in Table 1.

### 3.2 Effective Radius

The effective radius of a galaxy ( $R_e$ ) is the radius of the isophote containing half of the total luminosity (cf. Binney & Tremaine (2008) p. 21). The definition is simple in concept but much less simple to measure, because it requires discriminating data at both the inner galaxy, to determine the central profile, and at large galactocentric radii, to determine the outer limits of the galaxy profile. In addition, the results can be wavelength dependent due primarily to the relative contribution of young stars, old stars, and dust. Consequently, the effective radius values in the literature can differ considerably.

Since  $R_e$  is an essential piece in determining a galaxy’s  $M_\bullet$ ,  $M_{dyn}$ , and location in the fundamental plane we wanted to understand its uncertainty. In Figure 2 are plotted the values of  $R_e$  that we found for our galaxy sample. The values plotted were based on data from the literature adjusted to our distances as given in Table 1; adoption of the redshift-based distances would change the details but not the overall picture. It is important to note here that none of the  $R_e$  catalogues we used, except those from the 2MASS Extended Sources Catalogue (Skrutskie et al. 2006), contained all of our galaxies. In addition, the methods used are also very different. As seen in Figure 2, the range of  $R_e$  for a given galaxy can be almost a factor of two. Ideally the value of  $R_e$  for each galaxy would be based on detailed comparisons

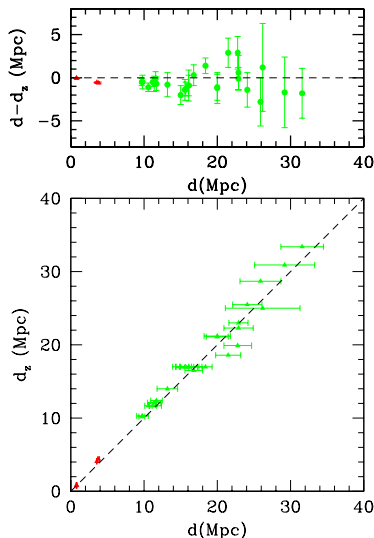


**Figure 1.** Comparison of redshift-based distances with those from stellar standard candles (red) and surface brightness fluctuations (green). In the upper panel the difference  $d - d_z$  is plotted against distances based on stellar indicators such as resolved stars and SBF. In the lower panel we plot  $d_z$ , the redshift-based distance, against the stellar-based value.

of available sources that take into account their strengths and limitations. But, because of the range of methods, limiting magnitudes, wavelength of the observations, and differing overlap, we decided to simply use the  $R_e$  given in the  $M_\bullet$  determination paper for each galaxy.

Note that the data shown are not meant to represent a complete list of all  $R_e$  data in the literature. Rather, this discussion is intended to show the range of values found for a given galaxy and act as a reminder that this quantity can be difficult to measure consistently.

### 3.3 Velocity Dispersion

A search of the HyperLeda (Paturel et al. 2003) database shows that published  $\sigma_e$  values also range widely, by even as much as  $\sim 100$  km/s or more for a single galaxy. McElroy (1995) compared results from different sources and tabulated velocity dispersions for more than 1500 galaxies based on his analysis of 85 standard galaxies. In Figure 3 the 15 McElroy standard galaxies in our sample are shown in red with the rest in green. Superimposed on the line for each galaxy are also the McElroy value (blue), the HyperLeda value (black \*) and the value quoted in the  $M_\bullet$  paper (black x). We note that, formally, the expected uncertainties in  $\sigma_e$  are often quoted as  $\leq 5\%$  (cf. Gebhardt 2004), but the scatter among different studies for the same galaxy is obviously much larger than that. The discordance between this

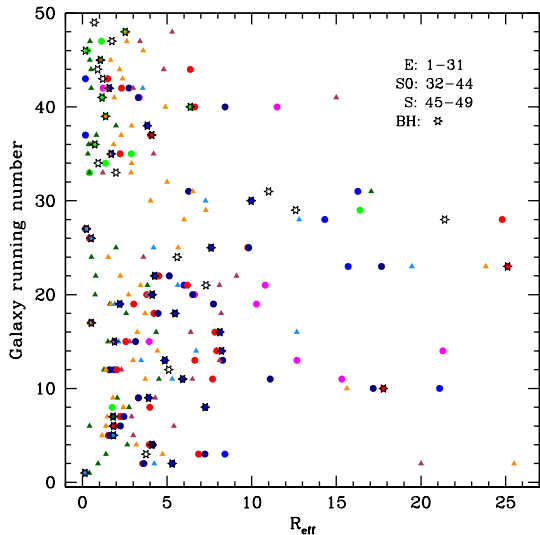


**Figure 2.** Values of  $R_e$  from various sources are plotted against running galaxy number. Filled circles are blue: Faber et al. (1989), green; Bassino et al. (2006), red: Lauer et al. (2007), magenta: Kormendy et al. (2009), navy blue: Hopkins et al. (2009). Filled triangles are maroon: Marconi & Hunt (2003), dark green: Hu (2008), dark orange: (2MASS), dodger blue: Magorrian et al. (1998). The black starred symbol is the value of  $R_e$  used in the determination of  $M_\bullet$ .

and the data plotted in Figure 3 suggests that observational factors such as spatial resolution, choice of  $R_e$ , and limiting magnitude are important but difficult to correct for in a given data set. Another way to compare the values in the literature is shown in Figure 4 where we have simply plotted the  $\sigma_e$  value adopted in the black hole mass determination (x-axis) vs. the HyperLeda and McElroy average values (y-axis). Interestingly, except for a few galaxies, the values are consistent within about twice the nominal  $\pm 5\%$  scatter usually adopted for  $\sigma_e$ . Thus, as with  $R_e$ , our tabulated values of  $\sigma_e$  are those used in the  $M_\bullet$  determination studies. We believe this makes the most sense when comparing galaxy parameters such as  $\sigma_e$ ,  $M_\bullet$ , and  $M_{dyn}$ .

### 3.4 Central Black Hole Masses

The number of galaxies with measurements of  $M_\bullet$  has increased significantly in the past decade and is now approaching 100, with more to come. Most of the data in Table 1 can be found in the compilations of Graham (2008), Gültekin et al. (2009b), and McConnell et al. (2011), supplemented by a few additional studies. Generally the masses we quote are from a single source, though a small number of galaxies have more than one determination. In the case of NGC 1399 we have used a weighted mean of the results from Gebhardt

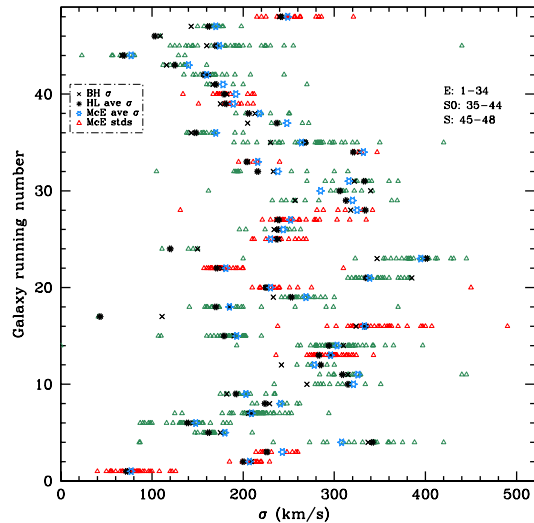


**Figure 3.** Plotted are velocity dispersion values from HyperLeda for the galaxies in our sample against running galaxy number. Open red triangles are McElroy “standard” galaxies and green triangles are the rest of the sample. The black X represents the velocity dispersion used in the black hole mass determination, the black asterisk is the average value from HyperLeda, and the open blue asterisk is the McElroy average for each galaxy.

et al. (2007) and Houghton et al. (2006). The case of NGC 5128 is somewhat more complex. Gültekin et al. (2009b) list  $M_\bullet = 7.0 \times 10^7 M_\odot$  from Cappellari et al. (2009) and  $3 \times 10^8 M_\odot$  from Silge et al. (2005), but choose to plot the latter on their  $M - \sigma$  relation. We have chosen to follow the reasoning of Neumayer et al. (2007) and Neumayer (2010), averaging the two values they provide based on stellar and gas dynamics. This smaller  $M_\bullet$  brings NGC 5128 into better agreement with the  $M - \sigma$  relation, but not for the  $N_{GC} - M_\bullet$  relation. Finally, the black hole mass for NGC 4486B (Kormendy et al. 1997) is an upper limit which is uncertain because of both its probable low mass and the galaxy’s asymmetric double nucleus. We include it here for completeness but do not use it in the correlations below.

### 3.5 Cluster Populations

The data in Table 1 for the total numbers of globular clusters  $N_{GC}$  are taken from the new HHA13 catalog, resulting in the addition of 12 more galaxies than used in HH. Although this is a considerably larger sample than in the initial discussions of either Spitler & Forbes (2009) or Burkert & Tremaine (2010), our list is still dominated by E galaxies.

The quoted uncertainties on  $N_{GC}$  in Table 1 differ quite a bit from one galaxy to another; typically they may be at the level of  $\pm 20\%$  or so but they depend very much on the

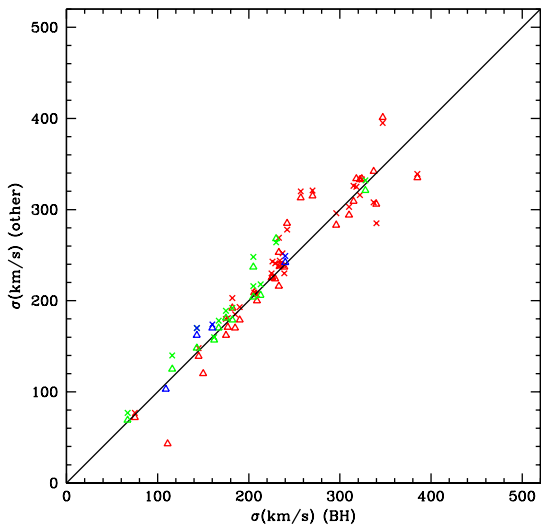


**Figure 4.**  $\sigma_e$  as used in the  $M_\bullet$  studies is plotted on the x-axis vs. mean values for  $\sigma_e$  from Hyperleđa (open triangles) and McElroy (x's) on the y-axis. E galaxies are shown in red, S0 in green and S in blue.

details of the individual photometric studies from which they were drawn. The uncertainties are relatively low in cases where the study had both wide area coverage and deep photometric limits reaching past the turnover point of the GC luminosity function. In these cases  $N_{GC}$  by definition is simply calculated as twice the total number of observed clusters brighter than the turnover point, summed over all galactocentric radii. In several other cases  $N_{GC}$  is derived from smaller-field coverage or photometric limits that fall short of the GCLF turnover, requiring larger extrapolations to estimate the total population. In some other cases such as for small satellites of nearby much larger galaxies (M32, NGC 4486B) only rough guesses can be made.

### 3.6 Bulge Mass

The final quantity listed in Table 1 is  $M_{dyn}$ , generally referred to as the virial bulge mass, given by

$$M_{dyn} = kR_e\sigma_e^2/G \quad (1)$$

where we use  $k=3$  instead of  $8/3$ , following Marconi & Hunt (2003). In the case of  $M_{dyn}$  we have not quoted formal uncertainties in Table 1, primarily because consistent observational uncertainties are not generally available for the values of  $R_e$  we have used. However, sample calculations based on typical observational uncertainties for  $R_e$  indicate that the resulting uncertainty in  $\log M_{dyn}$  is  $< 0.1$ . This is the value used in the statistical analyses described in section 4.

## 4 ANALYSIS

### 4.1 Reduced $\chi^2$ Estimator

Our first set of correlation solutions follows the method outlined in Tremaine et al. (2002) and Novak et al. (2006) and also used in HHA13. Briefly, if we assume data pairs  $(x_i, y_i)$  are related by  $y = \alpha + \beta x$  and that they have individual measurement uncertainties  $(\sigma_{x,i}, \sigma_{y,i})$ , then we minimize

$$\chi^2 = \sum \frac{(y_i - \alpha - \beta(x_i - \langle x \rangle))^2}{(\sigma_{y,i}^2 + \epsilon_y^2) + \beta^2(\sigma_{x,i}^2 + \epsilon_x^2)}. \quad (2)$$

Here,  $\epsilon_x$  and  $\epsilon_y$  represent any additional intrinsic or “cosmic” scatter over and above the nominal measurement uncertainties. If the quoted  $(\sigma_x, \sigma_y)$  values genuinely represent all the scatter present in the data, then we would have  $\epsilon_x = \epsilon_y = 0$ ; but if additional cosmic scatter exists, then the  $\epsilon$ 's can be adjusted upward from zero until we obtain a reduced  $\chi^2_\nu = 1$  from the fit. Of course, if we have only two parameters to correlate, it may be impossible to decide whether additional intrinsic scatter is in  $x$ , or in  $y$ , or in both. However, if we have several parameters to work with, it may be possible to find a self-consistent set of  $\epsilon$ 's for them all from the several 2-parameter correlations they allow.

Our first set of solutions, based on the data in Table 1 and listed in Table 2 below, assumes for each pair of parameters that  $\epsilon_x = 0$  and all the additional scatter (if any) is in  $y$ . That is,  $\epsilon_y$  is a free parameter adjusted to make  $\chi^2_\nu = 1$ . As is discussed at greater length in previous studies of this type (Tremaine et al. 2002; Novak et al. 2006, among others), including the  $\epsilon$  factor directly changes the relative weightings of the datapoints and thus noticeably influences the best-fitting slope  $\beta$ . The larger the adopted  $\epsilon$ , the more uniform the total weights of the datapoints become. The astrophysical importance is clearly that if we need to invoke nonzero  $\epsilon$ , then either the measurement uncertainties have been underestimated, or the galaxies do have an inbuilt variance that higher precision data would not remove.

In Table 2 the successive columns give (1) the pair of correlated quantities  $(y, x)$ ; (2,3) the galaxy types included in the fit and the number of individual datapoints; (4, 5, 6) the zeropoint  $\alpha$  and slope  $\beta$  of the fit, with internal uncertainties, and the sample mean  $\langle x \rangle$ ; (6) the residual rms scatter  $\sigma_y$  about the best-fit line; and (7) the added intrinsic scatter  $\epsilon_y$  needed to make the total goodness of fit  $\chi^2_\nu$  equal unity. The footnotes list individual galaxies excluded from each fit, either because of missing or uncertain data or because they are extreme outliers (these are more evident in the Figures shown below).

#### 4.1.1 $N_{GC}$ and $M_\bullet$ Versus Velocity Dispersion

The solutions in Table 2 exclude M32 (NGC 221), NGC 4486A, and NGC 4486B since the globular cluster numbers in those three dwarfs are small and extremely uncertain. However, all galaxies in Table 1 are plotted in Figures 5 and 6, which also show the solutions superimposed. The E-galaxy solution from 29 galaxies (including the outliers NGC 5128 and NGC 5845), is

$$\log N_{GC} = (2.825 \pm 0.071) + (4.120 \pm 0.540)(\log \sigma_e - 2.3)$$

and required invoking an extra dispersion  $\epsilon_y = 0.37$  to achieve  $\chi^2_\nu = 1$  and has a resulting rms scatter of  $\pm 0.383$

**Table 2.** Correlation Solutions from  $\chi^2$  Minimization

Solution For:	Sample	N	$\alpha$	$\beta$	$\langle x \rangle$	RMS $\sigma_y$	$\epsilon_y$	Note
log $N_{GC}$ vs log $\sigma_e$	E	29	$2.825 \pm 0.071$	$4.120 \pm 0.540$	2.30	0.383	0.37	6
	All	43	$2.821 \pm 0.055$	$3.720 \pm 0.382$	2.30	0.362	0.35	6
log $N_{GC}$ vs log $M_{dyn}$	E	31	$2.810 \pm 0.053$	$1.130 \pm 0.098$	11.0	0.295	0.23	1
	All	46	$2.932 \pm 0.047$	$0.870 \pm 0.068$	11.0	0.320	0.26	1
log $N_{GC}$ vs log $M_\bullet$	E	29	$2.952 \pm 0.059$	$0.840 \pm 0.080$	8.5	0.318	0.30	3
	E+S	33	$2.968 \pm 0.053$	$0.830 \pm 0.069$	8.5	0.302	0.27	4
	All	41	$2.968 \pm 0.050$	$0.750 \pm 0.047$	8.5	0.323	0.30	5
log $M_\bullet$ vs log $\sigma_e$	E	34	$8.413 \pm 0.080$	$4.730 \pm 0.539$	2.30	0.469	0.44	
	All	49	$8.412 \pm 0.067$	$4.610 \pm 0.403$	2.30	0.466	0.44	
log $M_\bullet$ vs log $M_{dyn}$	E	29	$8.497 \pm 0.060$	$1.010 \pm 0.083$	11.0	0.323	0.26	2
	All	44	$8.537 \pm 0.059$	$1.050 \pm 0.077$	11.0	0.393	0.34	
log $M_\bullet$ vs log $N_{GC}$	E	29	$8.33 \pm 0.064$	$0.930 \pm 0.097$	2.70	0.344	0.31	3
	E+S	33	$8.273 \pm 0.059$	$0.980 \pm 0.090$	2.70	0.340	0.30	4
	All	41	$8.221 \pm 0.062$	$1.070 \pm 0.092$	2.70	0.398	0.35	5

Notes: (1) Excludes M32, NGC 4486A, NGC 4486B  
(2) Excludes NGC 4486B, NGC 2778, NGC 4382, NGC 5128, and NGC 5845  
(3) Excludes M32, NGC 4486A, NGC 4486B, NGC 5128, NGC 5845  
(4) Excludes M32, NGC 4486A, NGC 4486B, NGC 5128, NGC 5845, Milky Way  
(5) Excludes M32, NGC 4486A, NGC 4486B, NGC 5128, NGC 5845, Milky Way, NGC 3414, NGC 4350  
(6) Excludes M32, NGC 4486A, NGC 4486B, NGC 2778, NGC 7457, and A2052

dex. The much larger database analyzed by HHA13 shows that the  $N_{GC}$  vs.  $\sigma_e$  correlation has similarly large scatter and in addition is highly nonlinear (see their Figure 7). For the SMBH masses, we also find for 34 E galaxies

$$\log M_\bullet = (8.413 \pm 0.080) + (4.730 \pm 0.539)(\log \sigma_e - 2.3)$$

with  $\epsilon_y = 0.44$  and for  $\chi_\nu^2 = 1$  a scatter of  $\pm 0.44$  dex. For comparison, in their original studies Ferrarese & Merritt (2000) found a slope of  $4.8 \pm 0.5$ , Gebhardt et al. (2000)  $3.75 \pm 0.3$ , and slopes in the range  $\simeq 4 - 5$  have been commonly quoted in later papers. We note that the absolute uncertainty in slope for this correlation is by far the largest for any we examined, though the *relative* uncertainty of 12% is similar to the others.

#### 4.1.2 $N_{GC}$ and $M_\bullet$ Versus Dynamical Mass

Again, the solutions in Table 2 exclude M32 (NGC 221), NGC 4486A, and NGC 4486B since the globular cluster numbers in those three dwarfs are small and extremely uncertain. The E-galaxy solution from 31 galaxies,

$$\log N_{GC} = (2.810 \pm 0.053) + (1.130 \pm 0.098)(\log(M_{dyn}/M_\odot) - 11.0)$$

required invoking an extra dispersion  $\epsilon_y = 0.23$  to achieve  $\chi_\nu^2 = 1$  and has a resulting rms scatter of  $\pm 0.295$  dex. For comparison, the solution found by HHA13 from 139 ellipticals with measured GCSs *excluding dwarfs* was  $N_{GC} \sim M_{dyn}^{1.035 \pm 0.033}$  with  $\epsilon_y = 0.28$  and rms scatter  $\pm 0.32$  dex. These two solutions are not significantly different, though the smaller and more highly selected sample used in this paper has a slightly smaller dispersion. Generally, we confirm HHA13 in that the total GC population of a (non-dwarf) galaxy is almost directly proportional to galaxy mass. The solution for these parameters is superimposed on the plot in Figure 7.

For  $M_\bullet$ , the solutions for either 29 E galaxies or 44 galaxies of all types are not significantly different. The larger sam-

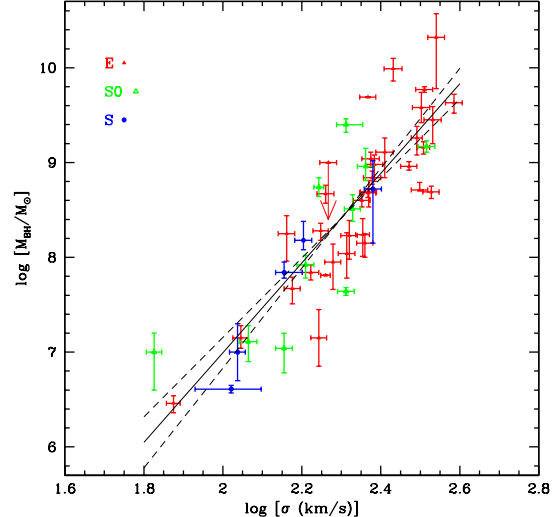


**Figure 5.** Plot of  $M_\bullet$  vs.  $\sigma_e$  for all 49 galaxies in our sample. E galaxies are in red filled triangles; S0 are green open triangles and S are filled blue circles. Overplotted is the  $\chi^2$  minimization solution for all 34 E galaxies.

ple (Table 2) gives

$$\log M_\bullet = (8.537 \pm 0.059) + (1.050 \pm 0.077)(\log(M_{dyn}/M_\odot) - 11.0)$$

with  $\epsilon_y = 0.34$  and a scatter of  $\pm 0.39$  dex; as with the other correlations, we have superimposed the solutions on the rel-

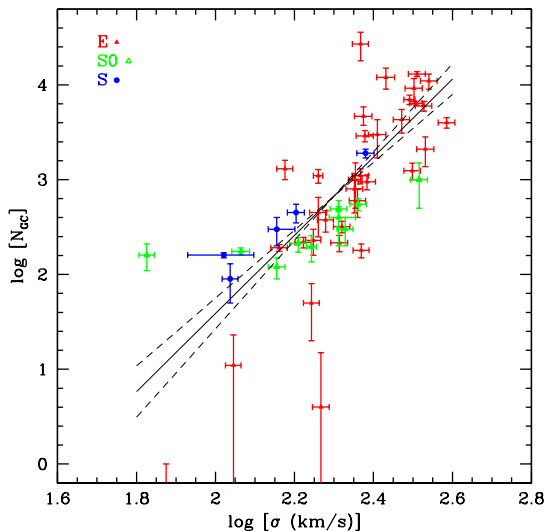


**Figure 6.** Plot of  $N_{GC}$  vs.  $\sigma_e$  for all 49 galaxies in our sample; symbols are as in Figure 5. Overplotted is the  $\chi^2$  minimization solution for 29 E galaxies.

evant data as shown in Figure 8. We find, as in previous studies, the same near-linearity for  $M_\bullet$  versus  $M_{dyn}$ . However, the residual dispersions and the required  $\epsilon_y$  are slightly larger than for  $N_{GC} - M_{dyn}$ .

#### 4.1.3 $N_{GC}$ Versus $M_\bullet$

Lastly, we plot  $N_{GC}$  vs  $M_\bullet$  and the inverse in Figures 9 and 10. For the “E+S” solutions which we view as the most reliable (excluding the S0 types whose apparent lack of correlation is not yet understood), we obtain

$$\log M_\bullet = (8.273 \pm 0.059) + (0.980 \pm 0.090)(\log N_{GC} - 2.7)$$

with  $\epsilon_y = 0.30$  and a scatter of  $\pm 0.34$  dex. For the inverse,

$$\log N_{GC} = (2.968 \pm 0.053) + (0.830 \pm 0.069)(\log M_\bullet - 8.5)$$

with  $\epsilon_y = 0.27$  and a scatter of  $\pm 0.30$  dex.

## 4.2 Optimized Solutions

With solutions in hand for several pairs of quantities selected from  $M_{dyn}$ ,  $N_{GC}$ ,  $M_\bullet$ , and  $\sigma_e$ , it should be possible in principle to determine a value of  $\epsilon$  (the cosmic scatter) for each one that would yield self-consistent solutions ( $\chi^2_\nu \simeq 1$ ) for every pair. After experimentation with different  $\epsilon$ ’s, we find that a self-consistent set is achieved near

$$\epsilon(\log M_{dyn}) = 0.2 \text{ dex;}$$

$$\epsilon(\log M_\bullet) = 0.25 \text{ dex;}$$

$$\epsilon(\log \sigma_e) = 0.07 \text{ dex;}$$

$$\epsilon(\log N_{GC}) = 0.2 \text{ dex.}$$

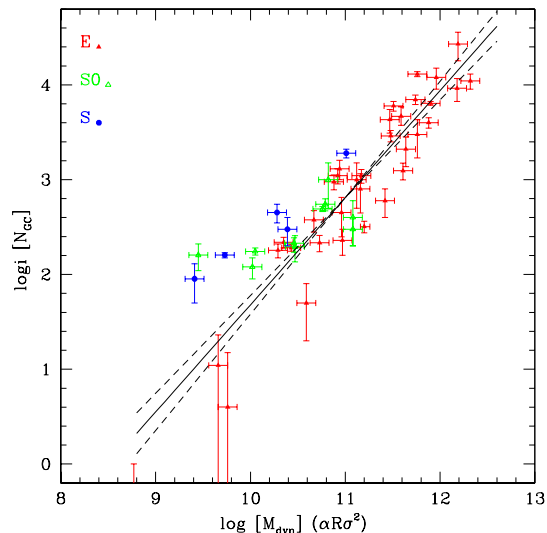


**Figure 7.** Plot of  $N_{GC}$  vs.  $M_{dyn}$  for all 49 galaxies in our sample; symbols are as in Figure 5. Overplotted is the  $\chi^2$  minimization solution for all 34 E galaxies.

We repeat that these are the additional scatters *over and above* the measurement uncertainties quoted in the literature that are needed to obtain correct  $\chi^2$ -minimization solutions. With these four ‘optimal’  $\epsilon$ ’s the resulting correlations are as given in Table 3.

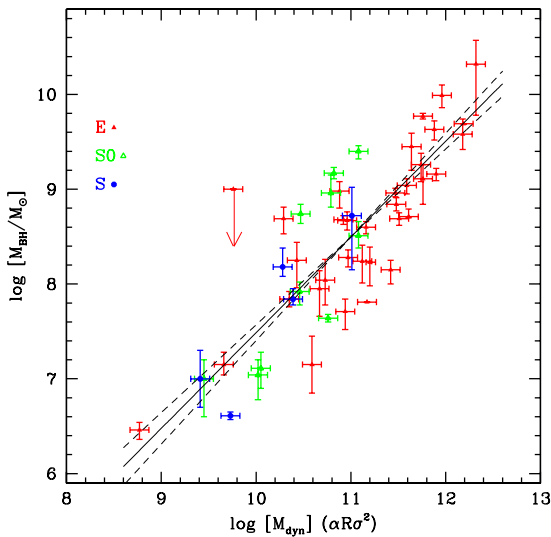
For each pair, we use the samples labelled “All” in Table 2. In some cases the best-fit slopes change noticeably from the solutions given in Table 2 (where we had put all the additional scatter into  $\epsilon_y$ ). These differences arise directly from the changes in the relative weightings of the datapoints when the assumed cosmic scatters are shared between the two quantities.

## 4.3 MCMC Analysis

To test for systematics in our fitting results, we perform a complementary analysis using a standard Monte-Carlo Markov Chain (MCMC) approach. We implement the Metropolis-Hastings method (Hastings 1970) using a codebase which has been well tested against a diverse range of problems in several published works (e.g. Poole et al. 2013; Mutch et al. 2013). Here, we present a number of solutions, each being a joint fit for the log-log slopes and intercepts of the  $M_{dyn} - N_{GC}$ ,  $M_{dyn} - \sigma_e$ ,  $M_\bullet - N_{GC}$ , and  $M_\bullet - \sigma_e$  relations. We use Eqn. 2 to calculate model likelihoods assuming that uncertainties in the observed properties presented in Table 1 are normally distributed for  $\sigma_e$  and  $N_{GC}$  and log-normally distributed for  $M_{dyn}$  and  $M_\bullet$ . In all cases, chains are calculated from  $10^5$  burn-in iterations and  $2 \times 10^6$  integration iterations. Proposal selection is optimised

**Table 3.** Optimized Solutions from  $\chi^2$  Minimization

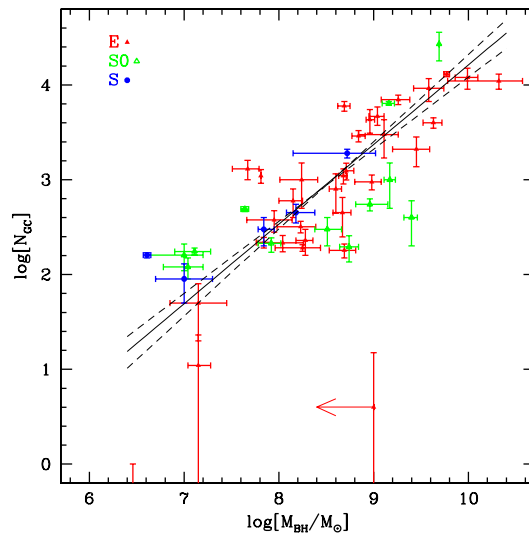
Solution For:	Sample	N	$\alpha$	$\beta$	$\langle x \rangle$	RMS $\sigma_y$
$\log N_{GC}$ vs $\log \sigma_e$	E	43	$2.790 \pm 0.062$	$4.600 \pm 0.088$	2.30	0.383
$\log N_{GC}$ vs $\log M_{dyn}$	E	46	$2.931 \pm 0.051$	$0.940 \pm 0.072$	11.0	0.295
$\log N_{GC}$ vs $\log M_\bullet$	E	41	$2.964 \pm 0.052$	$0.840 \pm 0.070$	8.5	0.318
$\log M_\bullet$ vs $\log \sigma_e$	E	49	$8.406 \pm 0.071$	$5.580 \pm 0.422$	2.30	0.469
$\log M_\bullet$ vs $\log M_{dyn}$	E	44	$8.541 \pm 0.061$	$1.140 \pm 0.079$	11.0	0.323
$\log M_\bullet$ vs $\log N_{GC}$	E	41	$8.185 \pm 0.063$	$1.190 \pm 0.027$	2.70	0.344

**Figure 8.** Plot of  $M_\bullet$  vs.  $M_{dyn}$  for all 49 galaxies in our sample; symbols are as in Figure 5. Overplotted is the  $\chi^2$  minimization solution for 29 E galaxies.

with a rotated covariance matrix computed iteratively pre-burn-in from 2000 proposals until all matrix elements converge to within 5%. Step sizes are selected to ensure a success rate of approximately 35% throughout.

All results presented in this section omit the Milky Way and NGC4486A,B for the same reasons given above. Lastly, all fits presented in this section have  $n_{Dof}=36$  degrees of freedom for which the  $p$ -value statistic rejects the null-hypothesis at a significance of  $\alpha(p) \leq 0.05$  for  $\chi^2/n_{Dof} \leq 50.997/36 = 1.42$ . We will use this throughout as our criterion for assessing the goodness of fit for the MCMC solutions.

To explore the idea that some or all of the uncertainties presented in Table 1 have been systematically underestimated or that the underlying relations host some degree of intrinsic scatter, we have applied this fitting procedure for various values of  $\epsilon_x$  and  $\epsilon_y$  for each relation. In the top panel of Figure 11 we present the influence of independently changing the value of  $\epsilon$  for each observable of interest ( $\epsilon_\sigma$ ,

**Figure 9.** Plot of  $N_{GC}$  vs.  $M_\bullet$  for all 49 galaxies in our sample; symbols are as in Figure 5. Overplotted is the  $\chi^2$  minimization solution for 29 E galaxies.

$\epsilon_{M_{dyn}}$ ,  $\epsilon_\bullet$ , and  $\epsilon_{N_{GC}}$ ) on the resulting reduced- $\chi^2$  and on the inferred slopes  $\beta$  for each relation. Since the effect of  $\epsilon_\sigma$  on relations involving  $M_{dyn}$  is mathematically equivalent to the effects of  $\epsilon_{M_{dyn}}$  through the relation  $\epsilon_{M_{dyn}} = 2\epsilon_\sigma + \epsilon_{R_e}$ , we present both on the same axis to compress our results. In this way, the effects of  $\epsilon_{M_{dyn}}$  can be interpreted in terms of underestimated uncertainties in  $\sigma$  (which carries through to estimates of  $M_{dyn}$  through Eqn. 1) or separately as intrinsic scatter or underestimated uncertainties in the measurement of  $M_{dyn}$ .

The results from these calculations agree generally well with those presented in the previous section: for every relation we find that fits of acceptable quality can only be achieved when  $\epsilon_x$  and/or  $\epsilon_y$  are significantly larger than zero. In addition the slopes  $\beta$  change with  $\epsilon$ , though how much a change is generated differs from one pair of parameters to another and sometimes moves in opposite directions for  $\epsilon_x$  and  $\epsilon_y$ .

For relations whose slope changes significantly with in-

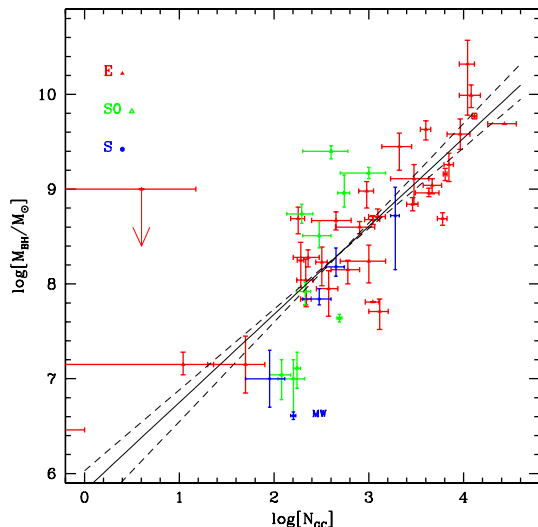


**Figure 10.** Plot of  $M_{\bullet}$  vs.  $N_{GC}$  for all 49 galaxies in our sample; symbols are as in Figure 5. Overplotted is the  $\chi^2$  minimization solution for 29 E galaxies.

creasing values of  $\epsilon_x$  or  $\epsilon_y$ , most of this change occurs at small initial displacements away from  $\epsilon = 0$ , converging to constant values by the time the  $\epsilon$ 's have increased sufficiently to permit a good fit. This trend is consistent with a scenario where a small number of precisely measured data points are dominating the fit. Our results suggest that  $\epsilon_{\sigma}$  is small ( $\leq 5\%$ ) while the other  $\epsilon$ 's need to be of the order of 10–30%. Moreover, covariance between our scaling relations demands that the  $\epsilon$ -values required for good fits in Figure 11 represent upper limits to what the lower limits of these values must be (since fits with  $\chi^2/n_{Dof} < 1.42$  are considered good as well).

Taking the values of  $\epsilon_{\sigma} \sim 0.05$ ,  $\epsilon_{\bullet} \sim 0.3$ ,  $\epsilon_{N_{GC}} \sim 0.2$  suggested by the top set of plots in this figure and iterating slightly for  $\epsilon_{M_{dyn}}$ , we have manually determined a self-consistent set of minimum values  $(\epsilon_{\sigma}, \epsilon_{\bullet}, \epsilon_{N_{GC}}, \epsilon_{M_{dyn}}) = (0.05, 0.30, 0.20, 0.1)$ . These particular values yield a good fit for each scaling relation of interest. In addition, these four values are encouragingly consistent with the optimal set of values we obtained in section 4.2 above through our  $\chi^2$  minimization solutions. This result is shown in the bottom set of plots in Figure 11 where we see that every relation converges to a good fit at approximately this set of values. The previous trends of  $\beta_{x-y}$  with  $\epsilon_x$  and  $\epsilon_y$  are still seen, but the amplitude of the dependence is generally reduced and the trends with  $\epsilon$  less severe. This dependence of  $\beta_{x-y}$  on  $\epsilon_x$  and  $\epsilon_y$  reliably moves in opposite directions for  $\epsilon_x$  and  $\epsilon_y$  now. And, furthermore, results for the slopes are insensitive to modest changes in the set of  $\epsilon$  values chosen. Finally and importantly, increases in the  $\epsilon$  values leading

to reduced- $\chi^2 \ll 1.42$  do not lead to significant changes of slopes.

The fits we derive using this set of optimal values for  $\epsilon$  are listed in Table 4 and are depicted in Figure 12. In each panel of the Figure, the heavy yellow line shows the optimal solution, with 68% and 95% confidence intervals shown as dark and light green shaded regions. Errorbars in black show the individual measurement uncertainties in the literature (no  $\epsilon$ 's added), while the effects of additional scatter are depicted in the blue errorbars. The heavy red line shows the best fit derived from  $\epsilon_x = 0$  for comparison, primarily to show how much the sharing of cosmic scatter among the parameters generates slope changes.

Notably, the addition of scatter (i.e. adopting the optimal solutions) has the effect of flattening all scaling relations involving the black-hole mass  $M_{\bullet}$ . This flattening is marginally significant at a  $\sim 68\%$  level in the case of the  $M_{\bullet}-\sigma$  and  $M_{\bullet}-N_{GC}$  relations, but is highly significant at  $\gg 95\%$  confidence for the  $M_{\bullet}-M_{dyn}$  relation. By contrast, the addition of scatter has no significant effect on the resulting slopes for relations involving  $N_{GC}$ .

Table 3 (classic  $\chi^2$  minimization) should be compared with Table 4 (MCMC fits). The differences in the  $\alpha$ -values are due simply to adoption of different zeropoint scalings. The more important comparison between the deduced slopes  $\beta$  reveals mutual agreement to within the combined uncertainties for most of the parameter pairs. Given the level of total scatter in all the relations, and the limitations in the still-small sample of galaxies, we suggest that the MCMC uncertainties on the slopes are likely to be the more realistic of the two methods. The largest discrepancy is nominally for  $N_{GC} - \sigma_e$  (slope 4.86 from Table 3, 6.11 from Table 4), but since the combined uncertainty is also large ( $\sim \pm 1.2$ ) the difference does not stand out especially when we also consider the presence of some individual outliers and the fact that the relation is intrinsically nonlinear (see again HHA13). The correlation for  $M_{\bullet} - N_{GC}$  yielded a noticeably flatter slope from MCMC ( $\simeq 0.81 \pm 0.2$ ) than from  $\chi^2$ -minimization ( $\simeq 1.19 \pm 0.03$ ), apparently because MCMC was less influenced by the dwarf-galaxy points appearing at the lower left of the graph.

The message we take from these comparisons is that there is no evidence at the present time to reject the view that  $M_{\bullet}$  and  $N_{GC}$  are rather closely directly proportional to one another. Both of these, in turn, scale almost exactly as  $M_{dyn}$ .

## 5 SUMMARY AND CONCLUSIONS

We have taken advantage of recent compilations of global parameters for galaxies in which the mass of the central black hole has been determined, and have combined these with a recent compilation of all galaxies with known globular cluster populations. We now find a sample of 49 galaxies which can be used to explore the  $M_{\bullet} - N_{GC}$  correlation that has attracted recent interest. For this set of galaxies we also have values of  $R_e$  and  $\sigma_e$  which can be used to examine correlations of  $M_{\bullet}$  and  $N_{GC}$  with  $\sigma_e$  and  $M_{dyn}$ .

Examining the raw data in detail, we find that particularly for  $R_e$  and  $\sigma_e$ , wide ranges of values for a given galaxy are often quoted in the literature that make it diffi-

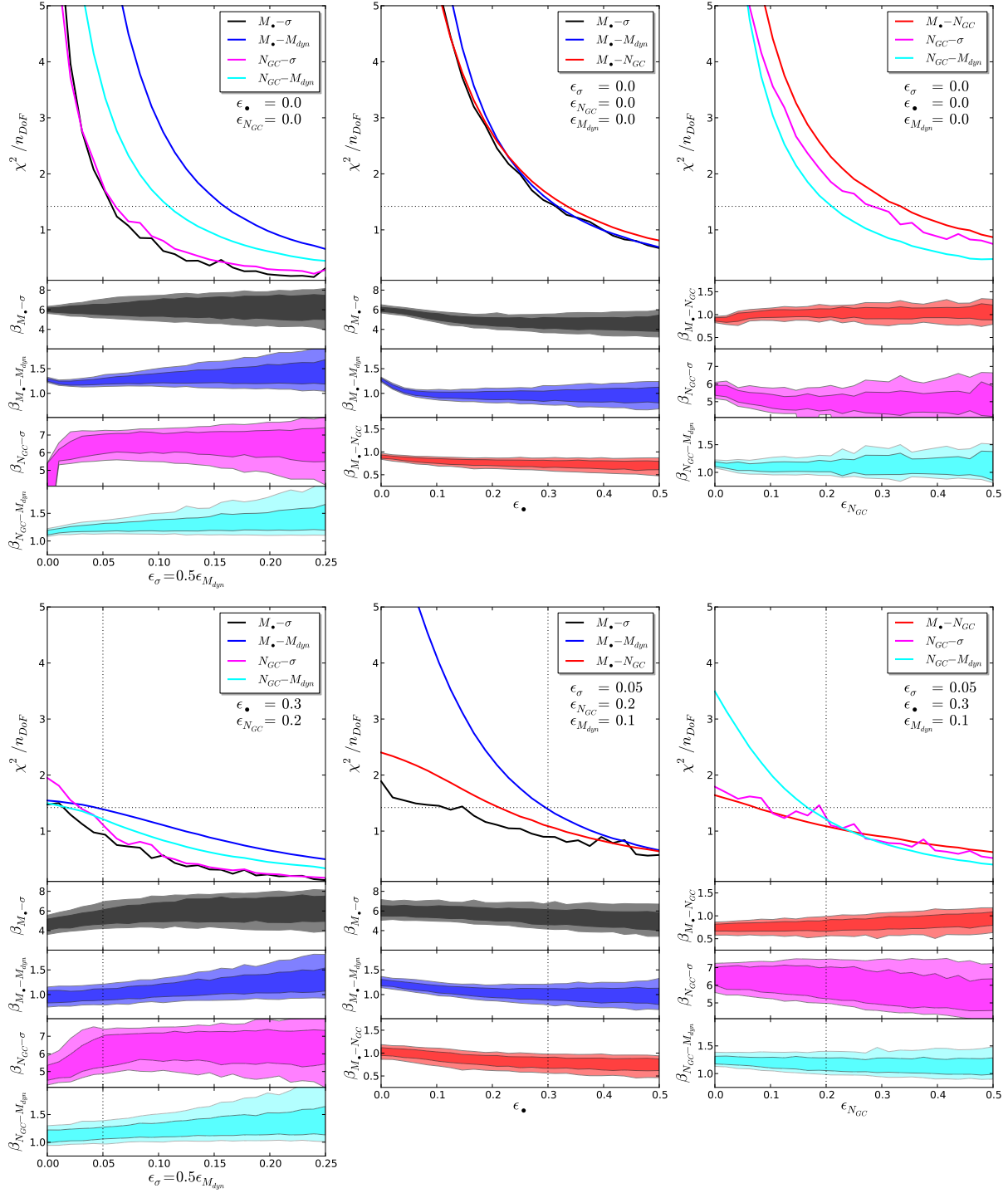


**Figure 11.** The effects of accounting for increased measurement uncertainties or intrinsic scatter on the goodness of fit and best-fit slopes of our 5 scaling relations of interest. Goodness of fit is expressed in the top frame of each column of plots (expressed in terms of reduced- $\chi^2$  for 36 degrees of freedom) with a horizontal dotted line depicting our good-fit criterion ( $\chi^2/n_{Dof} \leq 1.42$ ). The 68% and 95% confidence intervals for our best fit slopes are shown with dark and light coloured shaded regions respectively. The top set of plots shows the effect of each scatter variable ( $\epsilon_\sigma, \epsilon_{M_{dyn}}, \epsilon_{M_\bullet}$  or  $\epsilon_{N_{GC}}$ ) in isolation while the bottom set shows the same but for a self-consistent set of values permitting a good fit to every relation (indicated with vertical dotted lines). Since the effects of  $\epsilon_\sigma$  on relations involving  $M_{dyn}$  is mathematically equivalent to the effects of  $\epsilon_{M_{dyn}}$  through the relation  $\epsilon_{M_{dyn}} = 2\epsilon_\sigma$ , we present both on the same axis to compress our results.

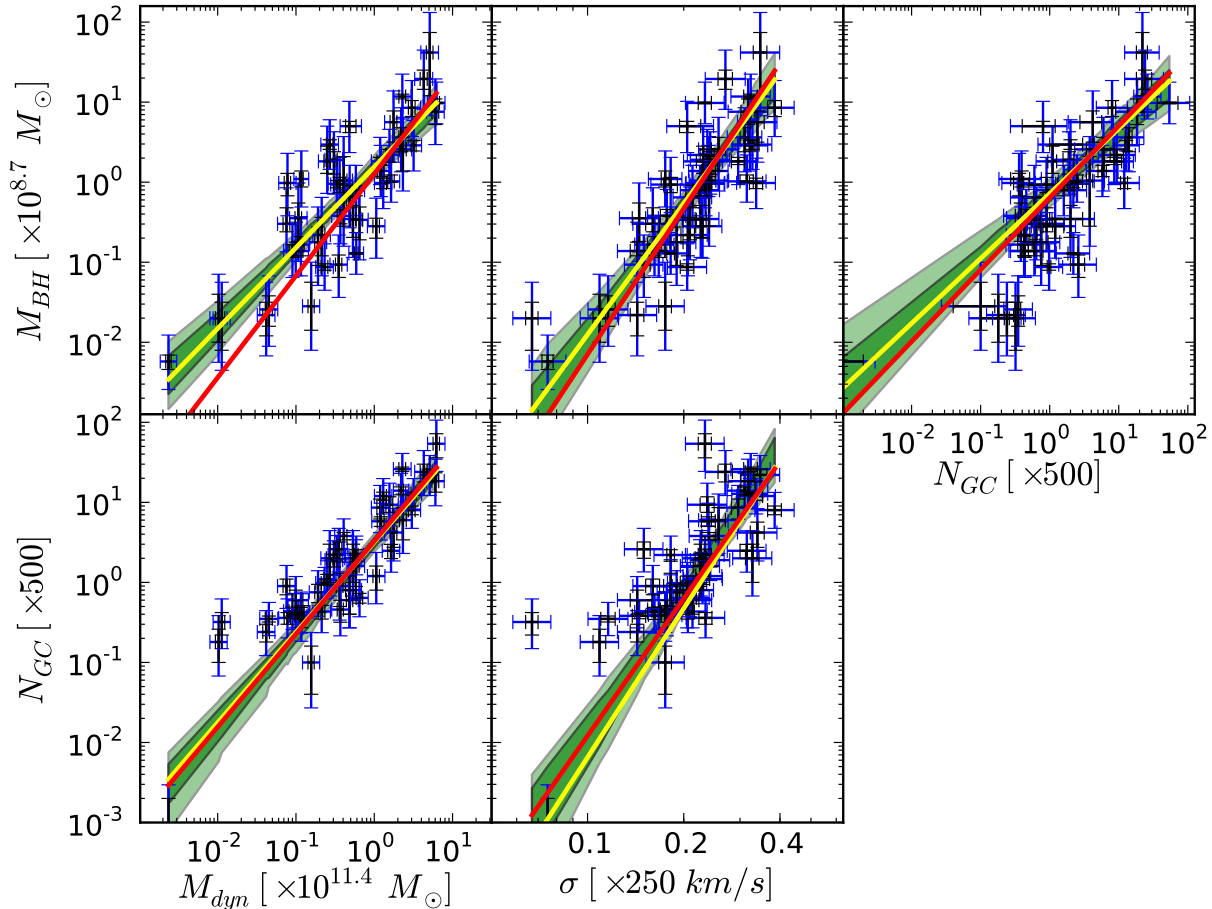


**Figure 12.** MCMC fits to the 2-parameter scaling relations. The upper panels show  $M_{\bullet}$  vs.  $M_{dyn}$ ,  $\sigma_e$ , and  $N_{GC}$ , while the lower panels show  $N_{GC}$  vs.  $M_{dyn}$  and  $\sigma_e$ . In each panel the yellow line marks the ‘optimal’ solution where both coordinates are allowed to have additional cosmic scatter and the shaded green areas mark the 68% and 95% confidence limits on the solution. The red line denotes the best-fit solution where only the y-axis is allowed to have additional scatter.

**Table 4.** Correlation solutions from our MCMC analysis. Unbracketed quantities are 68% confidence results and bracketed quantities are 95% confidence results.

Scaling Relation		$\alpha$	$\beta$
$\log N_{GC}$	vs $\log \sigma_e$	$4.29^{+0.49}_{-0.70}$ ( $+0.70$ $-0.94$ )	$6.11^{+0.90}_{-0.86}$ ( $+1.32$ $-1.24$ )
$\log N_{GC}$	vs $\log M_{dyn}$	$0.53^{+0.05}_{-0.09}$ ( $+0.11$ $-0.14$ )	$1.13^{+0.16}_{-0.07}$ ( $+0.28$ $-0.14$ )
$\log N_{GC}$	vs $\log M_{\bullet}$	$-0.14^{+0.11}_{-0.12}$ ( $+0.20$ $-0.20$ )	$0.81^{+0.10}_{-0.14}$ ( $+0.17$ $-0.25$ )
$\log M_{\bullet}$	vs $\log \sigma_e$	$3.58^{+0.40}_{-0.60}$ ( $+0.87$ $-0.88$ )	$5.36^{+0.76}_{-0.70}$ ( $+1.56$ $-1.16$ )
$\log M_{\bullet}$	vs $\log M_{dyn}$	$0.20^{+0.08}_{-0.11}$ ( $+0.15$ $-0.17$ )	$1.01^{+0.11}_{-0.12}$ ( $+0.20$ $-0.22$ )

cult to select best measurements. For these parameters we chose to use the values from the  $M_{\bullet}$  determinations as an attempt at consistency. All parameters were renormalized (where appropriate) to the Tonry et al. (2001) SBF galaxy distance catalogue as it contained virtually all of the galaxies in our sample and introduced no systematic biases within the quoted errors.

With the data available, we have solved for correlations

among the parameters  $M_{\bullet}$ ,  $N_{GC}$ ,  $\sigma_e$ , and  $M_{dyn}$  using both  $\chi^2$  minimization and Monte Carlo Markov Chain techniques.

- All the 2-parameter correlations show total scatters around the best-fit relations of  $\pm 0.3 - 0.4$  in the log. Both  $N_{GC}$  and  $M_{\bullet}$  follow tight and nearly linear relations particularly with  $M_{dyn}$  (bulge mass). Among all parameter pairs, the single relation with the lowest absolute scatter is  $N_{GC}$  versus  $M_{dyn}$ ; these two quantities scale accurately

in direct proportion, a result that we have also found from much larger galaxy samples (HHA13).

- One of our strongest findings is that in both fitting methods we must introduce additional variance  $\epsilon$  over and above the formal measurement uncertainties in order to obtain statistically valid solutions. To varying degrees these additional variances are needed in every one of the 4 parameters we use. The clear implication is that either the galaxy parameters have significant ‘cosmic scatter’, or (perhaps less likely) that the observational measurement uncertainties have been significantly underestimated. By using all of the 2-parameter correlations that are obtainable from the data, we find a self-consistent set of *extra variances* (in log scale) given by  $(\epsilon_\sigma, \epsilon_\bullet, \epsilon_{N_{GC}}, \epsilon_{M_{dyn}}) = (0.05, 0.30, 0.20, 0.1)$ . The  $M_\bullet$  values show the largest extra variance. As mentioned above, the need for additional variation in the correlation solutions is not new (e.g. Merritt & Ferrarese (2001), Tremaine et al. (2002), Novak et al. (2006) among others). What is new here is that the additional variance is required in all four parameters. For comparison we determined average measurement uncertainties for  $\sigma_e$ ,  $M_\bullet$ , and  $N_{GC}$  based on the data in Table 1. In this exercise we excluded the galaxies M32, NGC 4486A, and NGC 4486B (which were commonly left out of the correlation solutions) as well as NGC4374 and A2052 for which the quoted values of  $M_\bullet$  were upper limits only. We used  $\epsilon_{M_{dyn}} = 0.1$  as discussed in section 3.6. The variances for each parameter, based only on the quoted observational errors, are then  $(\epsilon_\sigma, \epsilon_\bullet, \epsilon_{N_{GC}}, \epsilon_{M_{dyn}}) = (0.02, 0.10, 0.19, 0.1)$  in the log. In all cases (except for  $\epsilon_{M_{dyn}}$ ), the *extra* variance required is more than twice the nominal observed values.

- The correlations involving  $M_\bullet$  have slopes that are more sensitive to the addition of  $\epsilon$ ’s than those involving  $N_{GC}$ ; the additional variance increases the relative importance of the smaller galaxies to the fit and ends up flattening all the slopes.

- The correlation of  $N_{GC}$  against  $\sigma_e$  is poorly constrained and (based on solutions from larger samples) more strongly nonlinear than the other parameter pairs.

At this stage of development, we suggest that the best observational route to exploring the  $N_{GC} - M_\bullet$  correlation further will be to reduce sample bias by adding more galaxies at lower luminosity, but especially by adding more S and S0 galaxies; at present, the E galaxies dominate the still-limited sample of galaxies in which both  $N_{GC}$  and  $M_\bullet$  are accurately measured.

The point of exploring these and other correlations among galaxy parameters is to gain an understanding of galaxy formation and evolution. All these parameters arise from the original mass concentration and gravitational potential well from which each galaxy formed. But each parameter examined here (as well as those such as galaxy luminosity, mass and halo mass among others) has evolved with time and in different ways, changing the interrelations as well. For instance,  $M_\bullet$  is expected to increase as gas and stars surrounding the galaxy centre are accreted and, in many cases this process is ongoing today. Contrarily  $N_{GC}$  will decrease with time as clusters are disrupted by both internal and external effects; but, in contrast to  $M_\bullet$ , most of the change in  $N_{GC}$  is expected to have happened within the first  $\sim 10^9$  years after formation.  $N_{GC}$  evolution is more smoothly pre-

dictable and due to the overall tidal field while  $M_\bullet$  evolution is more stochastic and can differ even between similar galaxies due to local differences in gas-rich merger histories. Thus, it is not surprising that  $M_\bullet$  relations have greater scatter than those involving  $N_{GC}$ . The physical scales at work are very different as well, from  $\sim 1$ pc for the central black hole to  $\sim 10^5$ pc for the globular cluster system. Since it is likely that most or all galaxy properties have changed over the past  $\sim 10^{10}$  years, then the nature of the various correlations today (their slope, linearity or curvature, and dispersion) will reflect *both* initial conditions and evolution to some degree.

Lastly, our results suggest that the dispersions observed in the various correlations are significantly affected by the individual evolutionary histories of the galaxies and cannot be explained by saying that the quoted uncertainties for the many galaxy properties are too small. We therefore favor the interpretation that the extra variances,  $\epsilon$ , introduced by both the reduced  $\chi^2$  and MCMC analyses are more likely to be reasonable estimates of the cosmic scatter.

## ACKNOWLEDGMENTS

This publication makes use of data products from the Two Micron All-Sky Survey which is a joint project of the University of Massachusetts and the Infrared Processing and Analysis Center/California Institute of Technology, funded by the National Aeronautics and Space Administration and the National Science Foundation.

We thank John Kormendy, Alister Graham, James Taylor, and Brian McNamara for helpful discussions. Much of this work was begun during an extended visit to Mount Stromlo Observatory (Australian National University). GP acknowledges support from S. Wyithe’s ARC Laureate Grant (FL110100072). WEH also acknowledges financial support through a grant from the Natural Sciences and Engineering Research Council of Canada. Lastly, we thank the referee for comments which helped improve the clarity of our discussion.

## REFERENCES

- Bassino, L.P., Faifer, F. R., Forte, J. C., Dirsch, B., Richtler, T., Geisler, D., & Schuberth, Y. 2006, *A&A*, 451, 798
- Battistini, P., Bonoli, F., Casavecchia, M., Ciotti, L., Federici, L., & Fusi-Pecci, F. 1993, *A&A*, 272, 77
- Bender, R. et al. 2005, *ApJ*, 631, 280
- Bicknell, G.V., Sutherland, R.S., van Breugel, W.J.M., Dopita, M.A., Dey, A., & Miley, G.K. 2000, *ApJ*, 540, 678
- Binney, J. & Tremaine, S. 2008, *Galactic Dynamics* (Princeton: Princeton University Press).
- Blakeslee, J. P., Tonry, J. L., & Metzger, M. R. 1997, *AJ*, 114, 482
- Blakeslee, J. P., Jordán, A., Mei, S., Côté, P., Ferrarese, L., Infante, L., Peng, E. W., Tonry, J. L., & West, M. J. 2009, *ApJ*, 694, 556
- Bower, G. A. et al. 1998, *ApJ*, 492, L111
- Bower, G. A. et al. 2001, *ApJ*, 550, 75
- Burkert, A. & Tremaine, S. 2010, *ApJ*, 720, 516 (BT)

- Brown, T. M., Ferguson, H. C., Smith, E., Kimble, R. A., Sweigart, A. V., Renzini, A., & Rich, R. M. 2004, *AJ*, 127, 2738
- Butterworth, S. J. & Harris, W. E. 1992, *AJ*, 103, 1828
- Cappellari, M., Neumayer, N., Reunanen, J., van der Werf, P. P., de Zeeuw, P. T. & Rix, H.-W., 2009, *MNRAS*, 394, 660
- Capuzzo-Dolcetta, R., & Donnaruma, I. 2001, *MNRAS*, 328, 645
- Capuzzo-Dolcetta, R., & Mastrobuono-Battisti, A. 2009, *AAp*, 507, 183
- Capuzzo-Dolcetta, R., & Vicari, A. 2005, *MNRAS*, 356, 899
- Chomiuk, S., Strader, J., & Brodie, J. P. 2008, *AJ*, 136, 234
- Croft, S. et al. 2006, *ApJ*, 647, 1040
- Dalcanton, J. J. et al. 2009, *ApJS*, 183, 67
- Dalla Bontà, E., Ferrarese, L., Corsini, E. M., Miralda-Escudé, J., Coccatto, L., Sarzi, M., Pizella, A., & Belfiori, A. 2009, *ApJ*, 690, 537
- Dirsch, B., Richtler, T., Geisler, D., Forte, J. C., Bassino, L. P., & Gieren, W. P. 2003, *AJ*, 125, 1908
- Djorgovski, S. & Davis, M. 1987, *ApJ*, 313, 59
- Emsellem, E., DeJonghe, H. & Bacon, R. 1999, *MNRAS*, 303, 495
- Faber, S. M., Wegner, G., Burstein, D., Davies, R., Dressler, A., Lynden-Bell, D., & Terlevich, R. J. 1989, *ApJS*, 69, 763A
- Fabian, A.C. 2012, *ARAA*, 50, 455
- Ferrarese, L., Ford, H. C., & Jaffe, W. 1996, *ApJ*, 470, 444
- Ferrarese, L. & Merritt, D. 2000, *ApJ*, 539, L9
- Ferrarese, L. et al. 2006, *ApJ*, 644, L21
- Fiorentino, G. et al. 2010, *ApJ*, 708, 817
- Forbes, D. A., Brodie, J. P., & Huchra, J. 1997, *AJ*, 113, 887
- Forbes, D. A., Georgakakis, A. E., & Brodie, J. A. 2001, *MNRAS*, 325, 431
- Gaibler, V., Khochfar, S., Krause, M., & Silk, J. 2012, *MNRAS*, 425, 438
- Gebhardt, K. & Kissler-Patig, M. 1999, *ApJ*, 583, 92
- Gebhardt, K. et al. 2000, *AJ*, 119, 1157
- Gebhardt, K., Adams, J., Richstone, D., Lauer, T. R., Faber, S. M., Gültekin, K., Murphy, J., & Tremaine, S. 2011, *ApJ*, 729, 119
- Gebhardt, K. 2004, Web-based catalog ([hoku.as.utexas.edu/~gebhardt/blackhole.html](http://hoku.as.utexas.edu/~gebhardt/blackhole.html)).
- Gebhardt, K. et al. 2007, *ApJ*, 671, 1321
- Ghez, A. M. et al. 2008, *ApJ*, 689, 1044
- Gillessen, S., Eisenhauer, F., Trippe, S., Alexander, T., Genzel, R., Martins, F., & Ott, T. 2009, *ApJ*, 692, 1075
- Giordano, L., Cortese, L., Trinchieri, G., Wolter, A., Colpi, M., Gavazzi, G., & Mayer, L. 2005, *ApJ*, 634, 272
- Graham, A. W., 2008, *PASA*, 25, 167
- Graham, A. W., Onken, C. A., Atahanassoula, E., & Combes, F. 2011, *MNRAS*, 412, 2211
- Grillmair, C. J. et al. 1996, *AJ*, 112, 1975
- Gültekin, K. et al. 2009a, *ApJ*, 695, 1577
- Gültekin, K. et al., 2009b, *ApJ*, 698, 198
- Gültekin, K., Tremaine, S., Loeb, A., & Richstone, D. O. 2011a, *ApJ*, 738, 17
- Gültekin, K., Richstone, D. O., Gebhardt, K., Faber, S. M., Lauer, T. R., Bender, R., Kormendy, J., & Pinkney, J., 2011b, *ApJ*, 744, 38
- Hanes, D. A. & Harris, W. E. 1996, *ApJ*, 304, 599
- Harris, G. L. H. 2010, *PASA*, 27, 475
- Harris, G. L. H., Rejkuba, M., & Harris, W. E. 2010, *PASA*, 27, 457
- Harris, G. L. H. & Harris, W. E. 2011, *MNRAS*, 410, 2347 (HH)
- Harris, W.E. 2009, *ApJ*, 699, 254
- Harris, W.E. 2010, *Phil. Trans. R. Soc. A*, vol. 368, no. 1913, 889
- Harris, W. E., Harris, G.L.H., & Alessi, M. 2013, *ApJ*, 772, 82 (HHA)
- Harris, W. E., Kavelaars, J. J., Hanes, D. A., Pritchett, C. J., & Baum, W. A. 2009, *AJ*, 137, 3314
- Harris, W. E., Pritchett, C. J., & McClure, R. D. 1995, *ApJ*, 441, 120
- Harris, W. E. & van den Bergh, S. 1981, *AJ*, 86, 1627
- Hastings W. K. 1970, *Biometrika*, 57, 97
- Tremonti, C., & White, Simon D. M. 2004, *ApJ*, 613, 109
- Hopkins, P., Lauer, T. R., Cox, T. J., Hernquist, L., & Kormendy, J. 2009, *ApJS*, 181, 486
- Hopp, U. et al 1995, *A&A* 296, 633
- Houghton, R. C. W. et al. 2006, *MNRAS*, 367, 2
- Hu, J. 2008, *MNRAS*, 386, 2242
- Ishibashi, W., & Fabian, A.C. 2012, *MNRAS*, 427, 2998
- Jalali, B., Baumgardt, H., Kissler-Patig, M., Gebhardt, K., Noyola, E., Lützgendorf, N., & de Zeeuw, P.T. 2012, *AAp*, 538, A19
- Jahnke, K. & Maccio, A. V. 2011, *ApJ*, 734, 92
- Jensen, J. B. et al. 2003, *ApJ*, 583, 712
- Johnson, C.I., Rich, R.M., Kobayashi, C., Kunder, A., Pilachowski, C.A., Koch, A., & de Propris, R. 2013, *ApJ*, 765, 157
- Jordán, A. et al. 2004, *AJ*, 127, 24
- Klamer, I.J., Ekers, R.D., Sadler, E.M., & Hunstead, R.W. 2004, *ApJ*, 612, 197
- Kormendy, J. 1988, *ApJ*, 335, 40
- Kormendy, J. & Richstone, D. O. 1995, *ARA&A*, 33, 581
- Kormendy, J., Bender, R., Magorrian, J., Tremaine, S., Gebhardt, K., Richstone, D., Dressler, A., Faber, S. M., Grillmair, C. J., & Lauer, T. R. 1997, *ApJ*, 482, L139
- Kormendy, J., Fisher, D. B., Cornell, M. E., & Bender, R. 2009, *ApJS*, 182, 216
- Kundu, A. & Whitmore, B. C. 2001, *AJ*, 121, 2950
- Larsen, S.S. & Brodie, J. P. 2000, *AJ*, 120, 2398
- Lauer, T. R. et al. 2007, *ApJ*, 664, 226
- Lee, M. G., Hwang, H. S., Kim, S. C., Park, H. S., Geisler, D., Sarajedini, A., & Harris, W. E. 2008, *ApJ*, 674, 886
- Magorrian, J. et al. 1998, *AJ*, 115, 2285
- Marconi, A. & Hunt, L. K. 2003, *ApJ*, 589, L21
- McConnachie, A. W., Irwin, M. J., Ferguson, A. M. N., Ibata, R. A., Lewis, G. F., & Tanvir, N. 2005, *MNRAS*, 356, 979
- McConnell, N. J. et al. 2011, *Nature*, 480, 215
- McElroy, D. B. 1995, *ApJS*, 100, 105
- Merritt, D. & Ferrarese, L. 2001, *ApJ*, 547, 140
- Mutch, S. J., Poole, G. B., & Croton, D. J. 2013, *MNRAS*, 428, 2001
- Neumayer, N. 2010, *PASA*, 27, 449
- Neumayer, N., Cappellari, M., Reunanen, J., Rix, H.-W., van der Werf, P. P., de Zeeuw, P. T., & Davies, R. I., 2007, *ApJ*, 671, 1329

- Novak, G. S., Faber, S.M., & Dekel, A. 2006, *ApJ*, 637, 96
- Nowak, N., Saglia, R. P., Thomas, J., Bender, R., Panella, M., Gebhardt, K., & Davies, R. I., 2007, *MNRAS*, 379, 909
- Nowak, N., Saglia, R. P., Thomas, J., Bender, R., Davies, R. I., & Gebhardt, K. 2008, *MNRAS*, 391, 1629
- Okon, W. M. M. & Harris, W. E. 2002, *ApJ*, 567, 294
- Olsen, K. A.G., Miller, B. W., Suntzeff, N. B., Schommer, R. A., Bright, J. 2004, *AJ*, 127, 2674
- Paturel, G. et al. 2003, *A&A*, 412, 45
- Peng, E. W. et al. 2008, *ApJ*, 681, 197
- Pignatelli, E., Salucci, P., & Danese, L. 2001, *MNRAS*, 320, 124
- Poole, G. B., Blake, C., Parkinson, D., et al. 2013, *MNRAS*, 429, 1902
- Peng, C. Y., 2007, *ApJ*, 671, 1098
- Puzia, T. H. et al. 2004, *A&A*, 415, 123 Goudfrooij, P., & Hempel, M. 2005, *A&A*, 439, 997
- Rauch, M., Becker, G.D., Haehnelt, M.G., Gauthier, J.-R., & Sargent, W.L.W. 2013, *MNRAS*, 429, 429
- Rekola, R., Richer, M. G., McCalla, M. L., Kaltonen, M. J., Kotilainen, J. K., & Flynn, C. 2005, *MNRAS*, 361, 330
- Rhode, K. 2012, *AJ*, 144, 154
- Richtler, T., Bassino, L. P., Dirsch, B., & Kumar, B. 2012, arXiv1203.1879R
- Rodríguez-Rico, C. A., Goss, W. M., Zhao, J.-H., Gómez, Y., & Anantharamaiah, K. R. 2006, *ApJ*, 644, 914
- Rusli, S. P., Thomas, J., Erwin, P., Saglia, R. P., Nowak, N., & Bender, R. 2011, *MNRAS*, 410, 1223
- Sadoun, R., & Colin, J. 2012, *MNRAS*, 426, L51
- Santiago-Cortés, M., Mayya, Y. D., & Rosa-González, D. 2010, *MNRAS*, 405, 1293
- Sarajedini, A., Mancone, C. L., Lauer, T. R., Dressler, A., Freedman, W., Trager, S. C., Grillmair, C., & Mighell, K. J. 2009, *AJ*, 138, 184
- Sarzi, M., Rix, H.-W., Shields, J. C., Rudnick, G., Ho, L. C., McIntosh, D. H., Filippenko, A. V., & Sargent, W. L. W. 2001, *ApJ*, 550, 65
- Schulze, A. & Gebhardt, K. 2011, *ApJ*, 729, 21
- Shen, J. & Gebhardt, K. 2010, *ApJ*, 711, 484
- Silge, J. D., Gebhardt, K., Bergmann, M., & Richstone, D. 2005, *ApJ*, 130, 406
- Silk, J. 2005, *MNRAS*, 364, 1337
- Silk, J., & Rees, M.J. 1998, *AAp*, 331, L1
- Skrutskie, M. F. et al. 2006, *AJ*, 131, 1163
- Snyder, G.F., Hopkins, P.F., & Hernquist, L. 2011, *ApJ*, 728, L24
- Spitler, L. R. & Forbes, D. A. 2009, *MNRAS*, 392, L1
- Spitler, L. R., Forbes, D. A., Strader, J., Brodie, J. P., & Gallagher, J. S. 2008, *MNRAS*, 385, 361
- Tamura, N., Sharples, R. M., Arimoto, N., Onodera, M., Ohta, K., & Yamada, Y. 2006, *MNRAS*, 373, 588
- Tonry, J. L. et al. 2001, *ApJ*, 546, 681
- Tremaine, S.D., Ostriker, J.P., & Spitzer, L. Jr. 1975, *ApJ*, 196, 407
- Tremaine, S. et al. 2002, *ApJ*, 574, 740
- Villegas, D. et al. 2010, *ApJ*, 717, 603
- Verolme, E. K. et al. 2002, *MNRAS*, 335, 517
- Wanger, A.Y., Bicknell, G.V., & Umemura, M. 2012, *ApJ*, 757, 136
- Wanger, A.Y., Umemura, M., & Bicknell, G.V. 2013, *ApJ*, 763, L18
- Willott, C. J. et al. 2010, *AJ*, 140, 546